JOURNAL OF MATERIALS SCIENCE 32 (1997) 4559–4573

Chemical reactivity of aluminium with boron carbide

J. C. VIALA, J. BOUIX
Laboratoire des Multimatériaux et Interfaces, UMR CNRS no. 5615, Université Lyon 1, 43 boulevard du 11 Novembre 1918, 69622 Villeurbanne Cedex, France

G. GONZALEZ
Instituto de Investigaciones en Materiales, UNAM, Apdo Postal 70-360, 04510 Mexico D.F., Mexico

C. ESNOUF
Groupe d'Etudes de Métallurgie Physique et de Physique des Matériaux, UMR CNRS no. 5510, INSA de Lyon, 69621 Villeurbanne Cedex, France

The chemical reactivity of boron carbide (B_4C) with metallic aluminium (Al) was studied at temperatures ranging from 900 to 1273 K (627–1000 °C). Al–B_4C powder mixtures were cold pressed, heated for 1–450 h under 10^5 Pa of purified argon and characterized by X-ray diffraction (XRD) optical metallography (OM), scanning electron microscopy (SEM) and electron probe microanalysis (EPMA). Whatever the temperature in the investigated range, B_4C has been observed to react with solid or liquid Al. As long as the temperature is lower than 933 K (660 °C), i.e. as long as Al is in the solid state, interaction proceeds very slowly, giving rise to the formation of ternary carbide (Al_3BC) and to diboride (AlB_2). At temperatures higher or equal to 933 K, Al is in the liquid state and the reaction rate increases sharply. Up to 1141 ± 4 K (868 ± 4 °C), the reaction products are Al_3BC and AlB_2: at temperatures higher than 1141 K, Al_3 BC is still formed while $Al_3B_{48}C_2$ (β-AlB_{12}) replaces AlB_2. In the three cases, interaction proceeds via the same mechanism including, successively, an incubation period, saturation of aluminium in B and C, nucleation and growth by dissolution–precipitation of Al_3BC and a C-poor boride and, finally, the passivation of B_4C by Al_3BC. These results are discussed in terms of solid–liquid phase equilibria in the Al–B–C ternary system, with reference to the binary invariant transformation: α-$AlB_{12} + L \Leftrightarrow AlB_2$, which has been found to occur at 1165 ± 5 K (892 ± 5 °C).

1. Introduction

With a low density ($d \approx 2.5$), a hardness just below that of diamond (9.5 + in Mohs' scale), excellent thermal stability and remarkable chemical inertness [1], boron carbide appears to be an interesting strengthening agent for aluminium based composites. It could more especially constitute an alternative to silicon carbide (SiC) for applications where a high stiffness or a good wear resistance are major requirements. Owing to the specific ability of the B_{10} isotope to capture neutrons, Al–B_4C composite materials may also find special applications in nuclear industries [2]. As boron carbide fibres have not been extensively developed, the studies reported on such materials mainly concern composites or cermets prepared from B_4C particles [3–6]. Besides these uses as reinforcing agents, boron carbide can also be deposited onto the surface of fibres in the form of a thin protective film. Such B_4C coatings were initially applied to 100 μm boron filaments and satisfactory results were generally obtained for aluminium based composites reinforced with these fibres [7]. More recently, a method for depositing a uniformly thin layer of B_4C on 5–10 μm carbon fibres by reactive chemical vapour deposition (RCVD) has been developed for a pilot plant in our laboratory [8–11]. One of the objectives of the research that is now being pursued is to employ these B_4C-coated carbon fibres for the reinforcement of aluminium alloys [12].

It is now well established that one of the keys to the development and application of high performance composite materials lies in subtle tailoring of the matrix–reinforcement interface that must combine an efficient load transfer with crack arrest capabilities. In metal matrix composites, the problem is complicated by the fact that most of the matrix–reinforcement couples of mechanical interest are out-of-equilibrium systems. As a consequence, the interface properties of materials based on such systems may be altered by the development of chemical reactions during processing or use. Thus, optimization of the strength, elastic modulus and toughness of these materials requires a thorough understanding of their interface chemistry.

0022–2461

As concerns the Al–B_4C interface chemistry, many questions remain unanswered for two main reasons. First, only a few studies on this subject are reported in the literature. Among these are a theoretical approach (based on thermodynamic calculations) of the phase equilibria in the ternary Al–B–C system by [13], a limited experimental study of the reaction at 1000 K of liquid aluminium with B_4C fibres [14] and more extensive investigations of the high temperature thermal behaviour of Al–B_4C cermets [4–6]: second, the results of these studies are in poor agreement. As an example, the thermodynamic calculations given in [13] indicate that B_4C and liquid Al should be in equilibrium at temperatures higher than 1155 K, while the results given in [4, 5] clearly show that Al and B_4C readily react up to at least 1673 K. Similarly, thermodynamic calculations indicate that Al and B_4C should react at 1000 K and give AlB_2 and the ternary compound $Al_8B_4C_7$; while the major phase reported with AlB_2 in the experiments realized at that temperature is either Al_4C_3 [14] or Al_4BC [4, 5], but never $Al_8B_4C_7$.

In this context, a general study was undertaken in our laboratory with the aim of clarifying the chemical reactivity of B_4C towards solid or liquid aluminium, at temperatures including the classical conditions for the elaboration of aluminium base matrix composites by liquid phase infiltration. After having prepared and characterized a new aluminium borocarbide with the chemical formula Al_3BC [15–17], we report in the present work the results of several series of isothermal diffusion experiments carried out at temperatures ranging from 900 to 1273 K on Al–B_4C and Al–B–C mixtures of different compositions. These results will be discussed in terms of reaction mechanisms, kinetics and thermodynamics.

1.1. Phases reported in the Al–B–C ternary system

Many phases containing Al, B and C are reported in the literature with various compositions and different crystal structures. Referring to recent reviews [18, 19] and to specific articles [20–31], we have listed in Table I the phases of the Al–B–C system whose existence can be considered as non-ambiguously established, with their thermal and structural characteristics when known.

As concerns the binary phases, we have not reported the compound Al_2B_3 (which decomposes above 798 K) because it very likely corresponds to a metastable phase that only appears in very special conditions [18]. As to the ternary phases, only four have been listed in Table I:

TABLE I Binary and ternary compounds reported in the Al–B–C system

Formula[a]	Thermal stability (K) and homogeneity range (h.r.)	Symmetry[c]	Unit cell parameters (nm)	Powder diffraction file [Reference No.]
Al_4C_3	Decomposes at 2429 narrow h.r.	Rhombohedral (*R*-3*m*)	$a = 0.33388$ $c = 2.4996$	35–799 [20, 21]
B_4C	Decomposes at 2723 $8.8 < C < 20$ at %	Rhombohedral (*R*-3*m*)	$a_{8.8} = 0.5672$ $c_{8.8} = 1.225$ $a_{20} = 0.5607$ $c_{20} = 1.209$	35–798 [1, 22, 23]
AlB_2	Decomposes at 1165[b] narrow h.r.	Hexagonal (P_6/mmm)	$a = 0.300\,54$ $c = 0.325\,28$	39–1483 [18, 24]
AlB_{12}	High temperature α-variety, decomposes at 2323	Tetragonal ($P4_12_12$ or $P4_32_12$)	$a = 1.016$ $c = 1.428$	12–640 [18, 25, 26]
	Low temperature γ-form	Orthorhombic ($P2_12_12_1$)	$a = 1.656$ $b = 1.753$ $c = 1.016$	[18, 24]
$Al_3B_{48}C_2$ ($\beta - AlB_{12}$)	High temperature form, decomposes near 2300	Tetragonal ($P4/nmm$)	$a = 0.882$ $c = 0.509$	19–269 [24, 27]
	Low temperature form A	Orthorhombic	$a = 1.234$ $b = 1.263$ $c = 0.508$	19–270 [24, 27]
	Low temperature form B	Orthorhombic	$a = 0.617$ $b = 1.263$ $c = 1.016$	19–271 [24, 27]
$AlB_{24}C_4$ (AlB_{10})	Decomposes above 2000	Orthorhombic (*Bbmm*)	$a = 0.8881$ $b = 0.9100$ $c = 0.5690$	15–617 [24, 28, 29]
$Al_8B_4C_7$ ($Al_8B_xC_6$)	Decomposes at 2110 $(2 < x < 4)$	Hexagonal ($P6_3/mcm$)	$a = 0.591\,18$ $c = 1.5915$	35–1216 [13, 30, 31]
Al_3BC (*X*, Al_4BC)	Stable up to at least 1273[b]	Hexagonal	$a = 0.6046$ $c = 1.1541$	[15, 17]

[a]Common denomination given in brackets below.
[b]Results determined from present work.
[c]Space group no. given in brackets below.

1. $Al_3B_{48}C_2$, often referred to as β-AlB_{12}, which can exist under three crystalline varieties (a high-temperature form and two low temperature forms).

2. $AlB_{24}C_4$, commonly designated as AlB_{10}, which decomposes into an Al-containing B_4C type phase at temperatures higher than about 2000 K [29].

3. $Al_8B_4C_7$ [30] also referred to as $Al_4C_4B_{1-3}$ [13] or $Al_8B_xC_6$, with $2 < x < 4$ [31].

4. Al_3BC, a ternary compound, which is the most recently characterized [15–17].

Phases such as $AlB_{12}C_2$ [29, 32] have not been reported in Table I because they are of the same structural type as B_4C and may therefore be considered as high temperature solid solutions of aluminium in this carbide [19].

As the ternary compound Al_3BC will appear to play an important role in the following discussion, some additional information on this phase will be recalled. First, we have observed that contrary to the three other aluminium borocarbides, this compound forms rather small crystals that rapidly decompose when they are immersed at room temperature in aqueous hydrochloric or hydrofluoric solutions ($3\,mol\,l^{-1}$). This may explain why it was not found in previous investigations where dissolution in such an aqueous solutions was generally employed to extract crystals from Al-rich melts. This is also why the first attempts to determine the symmetry and the cell parameters of this phase were made by exploiting powder XRD spectra recorded on samples in which the phase was mixed with aluminium in excess. At this stage, the strongest reflections observed were indexed as of hexagonal symmetry, with lattice parameters $a = 0.3491(2)$ nm and $c = 1.1541(4)$ nm $Z = 2$ [15]. Although the calculated and observed *d*-spacings were in very good agreement, some weak reflections remained unindexed [15]. In fact, complementary investigations by TEM and EPMA electron diffraction confirmed the hexagonal symmetry but revealed that the unit cell parameter, *a*, determined by X-ray diffraction had to be multiplied by a factor of $3^{1/2}$, leading to the definitive cell parameter values reported in Table II: $a_0 = 0.6046(4)$ nm, $c_0 = 1.1541(4)$ nm ($Z = 6$) and to the *d*-spacings indexation reported in Table III [16, 17]. It is not the subject of this paper to give a detailed description of the structural analysis that has been made to determine the space group and the atomic positions [17]. It will only be recalled here that strong arguments were obtained indicating that the new aluminium borocarbide we prepared and characterized as Al_3BC, the ternary compound referred to as phase *X* [4] and the compound Al_4BC [5, 33] actually correspond to the same phase.

TABLE II Analytical [15] and structural [16, 17] data for the new borocarbide Al_3BC

Chemical composition (at %)	Al: 60.9 ± 2 B + C = 39.1 ± 2 $0.45 < B/B + C < 0.55$
Symmetry	Hexagonal
Extinction group	*P–c–*
Possible space groups	$P6_3/mmc$, $P6_3/mcm$, $P6_3/mcc$
Lattice parameters, nm	
a	0.6046(4)
c	1.1541(4)
Cell volume, *V* (nm^3)	0.365
Mol $unit^{-1}$ cell, *Z*	6
Calculated density, *d*	2.829

2. Experimental procedure

Samples studied in this work were prepared from commercial powders of aluminium (purity 99.8 wt %; grain size, $d < 50$ μm, Alfa), boron (99.4 wt %, $d < 250$ μm, Alfa) carbon (spectrographic grade, $d < 25$ μm, Le Carbone Lorraine), boron carbide (stoichiometric B_4C with C traces, $d < 50$ μm, Riedel de Haën) and aluminium carbide (stoichiometric Al_4C_3, $d < 50$ μm, Alfa). Mixtures of these powders were ball-homogenized for 10 min in a tungsten carbide mortar and cold pressed either under 270 MPa into small parallelepipedic rods (with dimensions of $4 \times 6 \times 30$ mm; weight ≈ 2 g) or under 1 GPa into small cubes (edge = 6 mm; weight ≈0.4 g). These rods or cubes were then placed on alumina boats in

TABLE III X-ray power diffraction data for Al_3BC (*d*-spacings indexed and calculated for the unit cell parameter values $a = 0.6046$ nm and $c = 1.1541$ nm)

d (obs.) (nm)	*d* (calcul.) (nm)	I/I_0 (obs.) (%)	*h k l*	*d* (obs.) (nm)	*d* (calcul.) (nm)	I/I_0 (obs.) (%)	*h k l*
–	0.3878	< 5	1 0 2	0.1622	0.1623	5	1 1 6
0.3303	0.3023	5	1 1 0	0.1550	0.1550	< 5	2 0 6
0.2923	0.2924	100	1 1 1	0.14982	0.1499	10	2 2 1
0.2885	0.2885	15	0 0 4	0.14617	0.1462	10	2 2 2
0.2676	0.2678	60	1 1 2	0.1445	0.1447	< 5	1 1 7
0.2525	0.2527	10	1 0 4	0.1443	0.1443	< 5	0 0 8
0.2376	0.2377	75	1 1 3	–	0.1441	< 5	3 1 1
0.2087	0.2087	50	1 1 4	0.14067	0.1407	15	2 2 3
–	0.1979	< 5	1 2 0	–	0.1379	< 5	2 1 6
0.1949	0.1950	5	2 1 1	0.13391	0.1339	10	2 2 4
0.1923	0.1923	30	0 0 6	0.13022	0.1302	5	1 1 8
0.1871	0.1872	< 5	2 1 2	–	0.1297	< 5	1 3 4
0.1834	0.1835	35	1 1 5	0.12926	0.1292	30	3 0 6
0.1805	0.1805	< 5	1 0 6	0.12646	0.1264	10	2 2 5
0.1745	0.1745	70	3 0 0	0.11803	0.1180	5	1 1 9

a closed silica tube and heated to 900–1273 K under an atmospheric pressure of purified argon (10^5 Pa), using a classical horizontal tube furnace supplied by a stability controller. At the end of the isothermal heat treatment, the duration of which varied from 3 to 400 h, the silica tube was rapidly cooled in air (time constant at the order of 1 min).

After having verified that the weight losses were negligible, the resulting samples were characterized by XRD, OM, SEM and EPMA.

XRD spectra were systematically recorded on grossly polished faces of the treated rods, using a standard Philips equipment (PW 1720 generator, PW 1390 channel control unit, PW 1050 goniometer, Ni filtered CuK_α radiation at a wave length, λ, of 0.154 18 nm). This led to the determination of the crystalline nature of the phases present in the rods. Semi-quantitative analyses were also performed by this technique to evaluate the variations of the relative abundances of these phases as a function of the heating temperature or of the heating time. In that case, the size of the analysed samples, their positions in the X-ray beam and the operating parameters were rigorously controlled. For each phase characterized, the evaluation was realized by measuring the intensities of three characteristic diffraction lines free of overlap and by comparing the values thus obtained from one sample to another.

OM and SEM observations were made on sections of rods and cubes that were diamond polished to a finish of 1 μm. Examination by OM was useful to obtain rapidly a first idea of the constitution of the samples because the phases could be easily distinguished by their different colours: light grey for aluminium, dark grey for B_4C, bluish grey for Al_3BC, yellow for AlB_2 and brown with a shimmer of yellow for β-AlB_{12}. However, due to very large differences in hardnesses between these phases, obtaining good quality OM pictures at high magnification was a real problem and SEM was generally used for detailed observations (Hitachi S800 microscope).

Further characterization of the phases present in the samples was performed by EPMA, using a Cameca Camebax apparatus equipped with a wavelength dispersive spectrometer and an energy dispersive analyser. An accelarating voltage of 5 kV, a regulated beam current of about 30 nA and a counting time of 10 s were selected as standard operating parameters. For each phase analysed, the counting rates simultaneously recorded for Al, B and C in at least ten different points were averaged, substracted for the background, referred to the counting rates recorded under the same conditions on simple or complex standards (Al, B, C, AlB_2, Al_4C_3, B_4C, SiC) and finally corrected for atomic number, absorption and fluorescence (suppressed).

3. Results

Systematic experiments were undertaken in order to determine the influence of three parameters, heating temperature, composition of the Al–B_4C mixture and heating time, on the chemical reactivity of B_4C with aluminium. This was achieved by varying one of these parameters and fixing the two others (see Sections 3.1.–3.3.). Section 3.4. is devoted to the description of additional experiments aimed on the determination of phase equilibria in the Al–B–C system. The positions in the Al–B–C compositional triangle of the different mixtures prepared, with the corresponding experiment number, are indicated in Fig. 1.

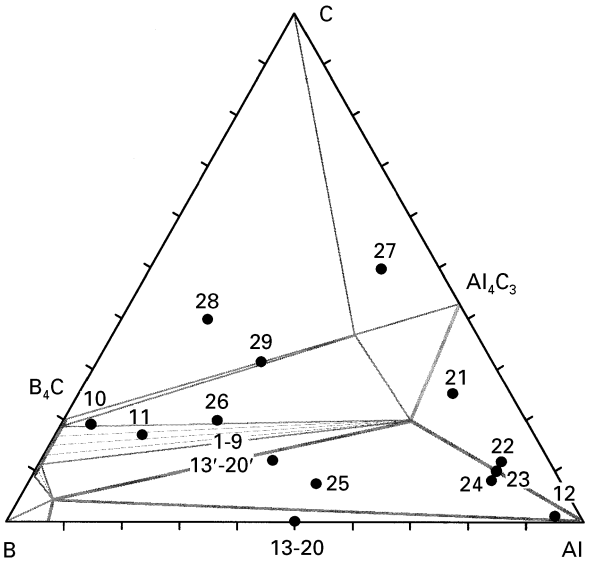

Figure 1 Position, in the Al–B–C compositional triangle, of the different mixtures studied in the present work (grey, dashed lines represent tie lines further constructed, see Fig. 14).

3.1. Phases characterized in Al–B_4C mixtures reacted for 160 h at 900–1273 K

In a first series of experiments, Al–B_4C rods having a fixed atomic composition of Al:B:C = 40:48:12 (in at %) were heated for a constant duration of 160 h at different temperatures ranging from 900 to 1273 K and rapidly cooled. Results obtained by XRD on these mixtures are reported in Table IV and Fig. 2: in Table IV are listed the phases characterized after heat treatment at different temperatures; in Fig. 2 are plotted the variations with reaction temperature of the relative abundances of these phases, as evaluated from the intensities of their characteristic XRD lines. It is worth noting that, except for the mixtures heated at

TABLE IV Phases characterized by XRD in Al–B_4C mixtures (Al:B:C = 40:48:12 at %) reacted for 160 h at temperatures ranging from 900 to 1273 K

Experiment no.	Temperature (K)	Phases characterized by XRD after heat treatment
1	900	Al, B_4C
2	920	Al, B_4C
3	950	Al, B_4C, Al_3BC, AlB_2
4	1000	Al, B_4C, Al_3BC, AlB_2
5	1050	Al, B_4C, Al_3BC, AlB_2
6	1100	Al, B_4C, Al_3BC, AlB_2
7	1150	Al, B_4C, Al_3BC, $Al_3B_{48}C_2$
8	1200	Al, B_4C, Al_3BC, $Al_3B_{48}C_2$
9	1273	Al, B_4C, Al_3BC, $Al_3B_{48}C_2$

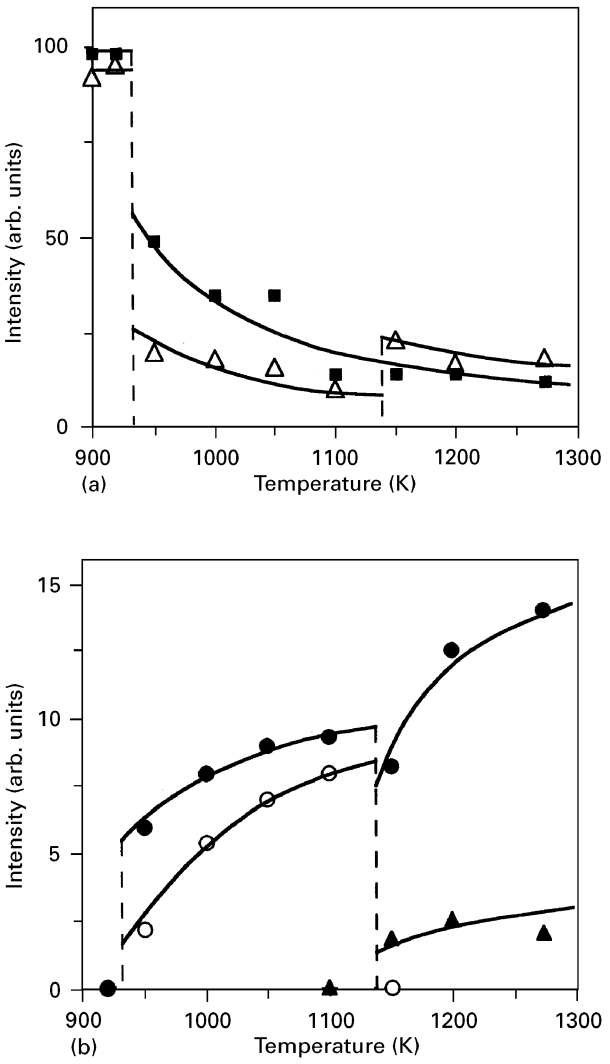

Figure 2 Relative abundances of reactants (a) and products (b) in Al–B_4C mixtures (Al:B:C = 40:48:12 at %) after heating for 160 h at 900–1273 K: (■) B_4C, (△) Al, (●) Al_3BC (○) AlB_2, (▲) $Al_3B_{48}C_2$.

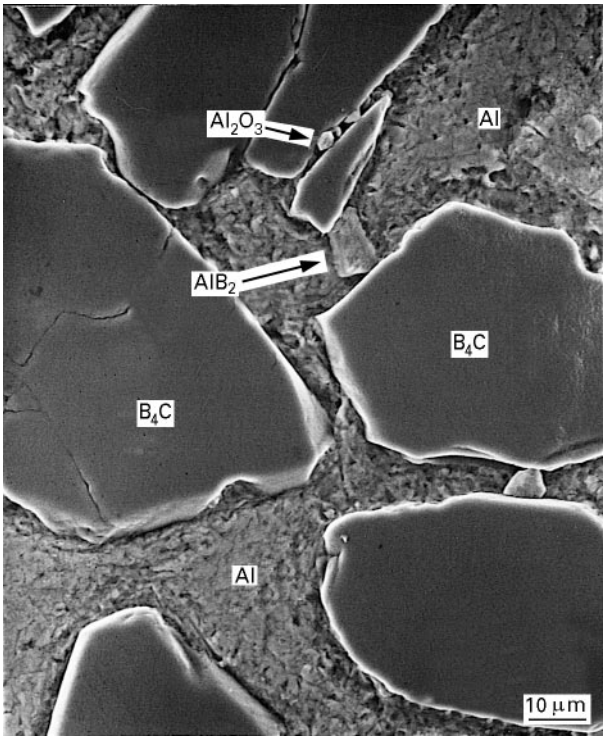

Figure 3 SEM photograph of an Al–B_4C sample (Al:B:C = 40:48:12 at %) heated for 160 h at 900 K (B_4C and Al are the major constituents and no solid state interaction can be detected).

900 and 920 K, interpretation of the XRD spectra of this series is non-ambiguous. Effectively, all the diffraction lines detectable in the different spectra recorded could be attributed to one of the reported phases and no reflection remained unindexed. In particular, after systematic refinement using a classical least squares programme, the unit cell parameters of the compounds characterized were found to be consistent with the literature data listed in Table I.

After heating for 160 h at 900 or 920 K, i.e. at temperatures just below the melting point of pure aluminium ($T_{m_{Al}} = 933$ K), B_4C and aluminium were the only two phases that could be characterized by XRD (Table IV). In addition to the characteristic reflections of these two phases, three extra lines were detected at angular positions corresponding to the three strongest reflections of the ternary carbide Al_3BC. Nevertheless, these lines were too weak to assure the presence of this carbide in the samples. As for Al_4C_3, AlB_2 or any other reaction product, no indication at all of their presence was obtained from XRD. SEM observations and EPMA analyses confirmed that samples heated for 160 h at 900 or 920 K mainly consisted of a porous aluminium matrix and of B_4C particles having the same morphologies as those of the grains of the starting B_4C powder, without any indication of the formation of a reaction zone at the metal carbide interface (Fig. 3). Crystals of the phase Al_3BC were searched for, but were not found; while small AlB_2 crystals were detected in rare places in the aluminium matrix, beside some Al_2O_3 impurity particles: these two sorts of crystals are marked on Fig 3.

By contrast with the foregoing observations, XRD results obtained after heating an Al–B_4C mixture for 160 h at 950 K, i.e. at a temperature just above the melting point of pure aluminium, clearly demonstrated that chemical interaction had occurred. Effectively, more than half of the Al and B_4C reactants were consumed, whereas substantial amounts of Al_3BC and AlB_2 were produced (Table IV, Fig. 2). These reaction products can be observed in the SEM photograph presented in Fig. 4. Al_3BC forms aggregates of small crystals surrounding the remaining B_4C particles, whereas AlB_2 appears as large faceted crystals with hexagonal shapes, most often embedded in the aluminium matrix.

As the heating temperature increased from 950 to 1100 K (for a constant heating time of 160 h), the relative abundance of each Al and B_4C reactant regularly decreased, while that of the Al_3BC and AlB_2 reaction products increased, as shown in Fig. 2. Results reported in this figure also indicate that Al was consumed in greater amounts than B_4C. As a consequence, the sample heated for 160 h at 1100 K mainly consisted of three phases, AlB_2, Al_3BC and B_4C, as confirmed by SEM observations (Fig. 5).

At a heating temperature of 1150 K, the aluminium diboride AlB_2 no longer formed. The products

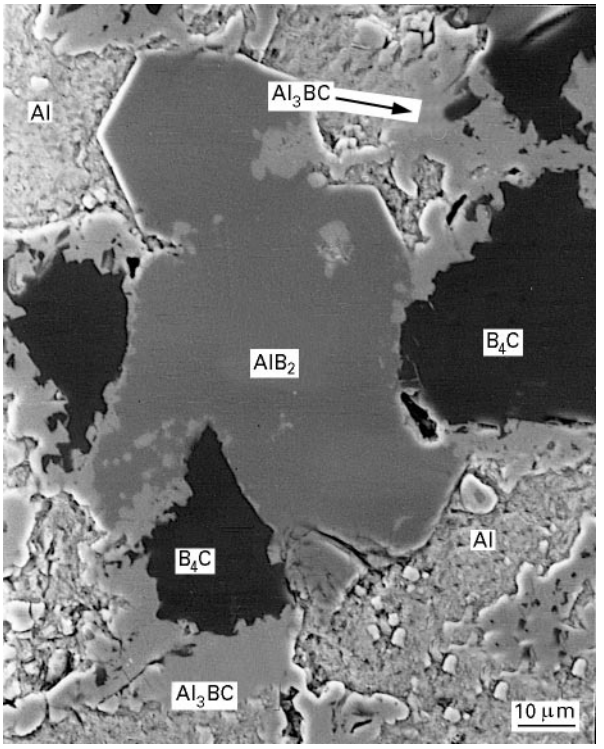

Figure 4 Al–B_4C sample (Al:B:C = 40:48:12 at %) heated for 160 h at 950 K (formation of Al_3BC and AlB_2 by reaction of B_4C with liquid Al is clearly visible).

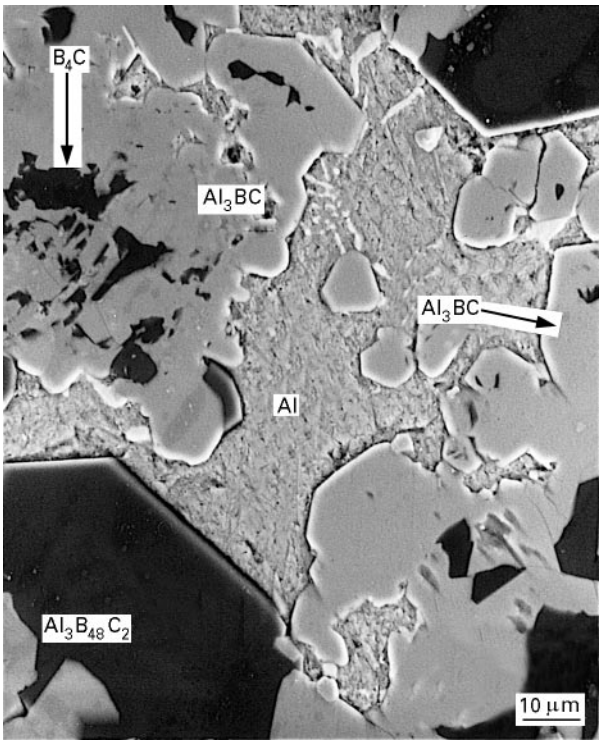

Figure 6 Al–B_4C sample after heating for 160 h at 1273 K [Al_3BC, $Al_3B_{48}C_2$ (β-AlB_{12}) and metallic aluminium are the major constituents (B_4C tends to disappear)].

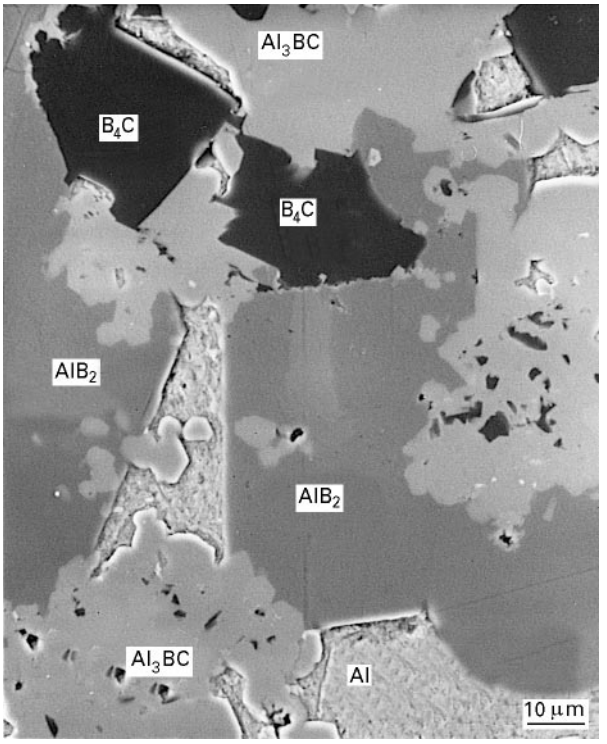

Figure 5 SEM photograph of an Al–B_4C sample (Al:B:C = 40:48:12 at %) reacted for 160 h at 1100 K (AlB_2, Al_3BC and B_4C are the major constituents; Al tends to disappear).

characterized after 160 h reaction were the ternary carbide Al_3BC (the most abundant) and the aluminium borocarbide $Al_3B_{48}C_2$ (β-AlB_{12}, low temperature forms A + B). Moreover, it was observed that a larger quantity of metallic aluminium remained at 1150 K than at 1100 K, whereas the amounts of B_4C consumed were about the same at the two temperatures (Fig. 2). This tendency for liquid aluminium to remain with the reaction products in the samples heated at temperatures higher or equal to 1150 K was confirmed by the XRD results obtained after heating at 1200 and 1273 K (Fig. 2) and by the SEM observations made on the corresponding Al–B_4C samples. As an illustration, it is clear from the SEM photograph presented in Fig. 6 that B_4C tends to be entirely consumed after heating for 160 h at 1273 K with Al and that Al_3BC, $Al_3B_{48}C_2$(β-AlB_{12}) and metallic aluminium are the major constituents of the treated sample.

At the end of this first series of experiments, three different temperature ranges could be distinguished concerning the chemical behaviour of boron carbide in the presence of aluminium:

1. A low temperature range where chemical interaction between solid aluminium and B_4C was not obvious after heating for 160 h.

2. A medium temperature range extending from 933 K to about 1100 K where liquid aluminium and B_4C readily reacted to give the ternary carbide Al_3BC and the aluminium diboride AlB_2.

3. A high temperature range extending from about 1150 K to at least 1273 K where B_4C decomposed into Al_3BC and $Al_3B_{48}C_2$ (β-AlB_{12}).

3.2. Influence of the Al:B_4C ratio

Experiments were realized by heating for 160 h at 1000 and 1273 K Al–B_4C mixtures having the Al:B:C compositions of 5:76:19 at %, 15:68:17 at % (B_4C-rich) and 95:4:1 at % (Al-rich) for 160 h at 1000 and 1273 K. In Fig. 1, these mixtures correspond to the

points marked 10, 11 and 12, respectively. Analyses revealed that these samples all consisted of the same phases as those previously characterized (of course, their relative abundances varied considerably). More especially, unreacted aluminium and B_4C were systematically present with Al_3BC and AlB_2 or $Al_3B_{48}C_2$ (β-AlB_{12}) after heating at 1000 or 1273 K, respectively, and this whatever the Al–B_4C ratio. In other words, for a heating time of 160 h, reaction did not go to completion either at 1000 or at 1273 K.

3.3. Influence of the heating time

In order to obtain more detailed information on the kinetics and the mechanism of chemical interaction between boron carbide and aluminium, Al–B_4C mixtures were prepared, cold pressed and heat treated for varying times at 920, 1000 and 1273 K, each temperature being representative of one of the three ranges previously distinguished. After rapid cooling, the resulting samples were characterized by XRD, SEM and EPMA. XRD studies were carried out on Al–B_4C parallelepipedic rods having the same atomic compositions as in Section 2, i.e. Al:B:C = 40:48:12 at % (points 1–9 in Fig. 1). SEM observations and EPMA analyses of the reaction zones at the Al–B_4C interface were made on Al-rich Al–B_4C cylinders having their initial compositions fixed at Al:B:C = 95:4:1 at % (point 12 in Fig. 1).

At the lowest of the three temperatures, 920 K, the main question was to decide whether reaction was possible between B_4C and solid aluminium (T_{mAl} = 933 K). To clear up this point, an Al–B_4C rod and an Al–B_4C cylinder were heat treated at that temperature for 450 h (instead of 160 h as in Section 2). In this case, the ternary carbide (Al_3BC) and the aluminium diboride (AlB_2) were unambiguously characterized by XRD and EPMA in the treated samples, in addition to unreacted B_4C, metallic aluminium and Al_2O_3 inclusions. In the SEM photograph of the Al-rich cylinder presented in Fig. 7, the ternary carbide Al_3BC appears as small crystals (d = 1–3 μm) located at the interface between the B_4C particle and the aluminium matrix. In some places, these crystals have already joined together forming a quasi-continuous reaction zone. In other places, metallic aluminium is still in direct contact with the surface of the B_4C particle. As for AlB_2, crystals of this phase (d = 5–10 μm) appear embedded in the aluminium matrix, sometimes far from the Al–B_4C interface. It was thus established that B_4C can effectively decompose into Al_3BC and AlB_2 by reaction with solid aluminium. Moreover, on account of the duration of the experiment (450 h) and temperature (just 13 K below the melting point of pure aluminium), it is clear that this solid state decomposition will always proceed at a very slow rate.

Al–B_4C rods and cylinders were also heat treated at 1000 K with increasing time from 3 to 400 h. At this temperature, the reaction products were always Al_3BC and AlB_2. Fig. 8 shows the variation, with the square root of the reaction time ($t^{1/2}$), of the relative abundances of the reactants Al and B_4C (Fig. 8a) and

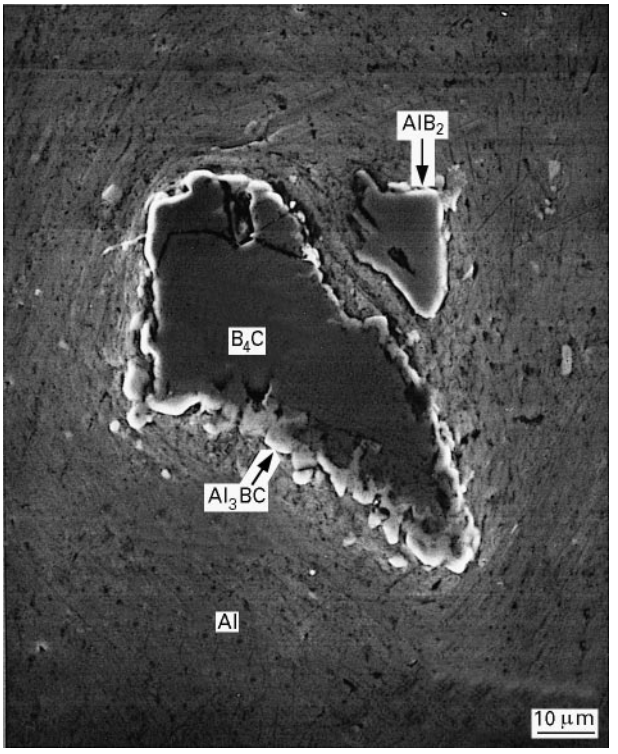

Figure 7 SEM photograph of an Al–B_4C sample (Al:B:C = 95:4:1 at %) heated for 450 h at 920 K, showing the growth of Al_3BC and AlB_2 crystals by solid state reaction between Al and B_4C.

of the products Al_3BC and AlB_2 (Fig. 8b), as determined by exploitation of the XRD data recorded on Al–B_4C parallelepipedic rods. The series of SEM photographs presented in Fig. 9a–f illustrates the morphological changes that occurred at the metal–carbide interface when the reaction time increased from 3 to 400 h.

With the reserves previously enunciated concerning the quantitative exploitation of XRD data, it could be assumed from the results plotted in Fig. 8 that processes of two different kinds were successively controlling the kinetics of the isothermal decomposition of B_4C by liquid aluminium at 1000 K. At the beginning of the interaction (following less than $\sim$15 h reaction), the amounts of reactants consumed and of products formed appeared to vary rapidly and quasi-linearly with the reaction time (parabola branches in Fig. 8). Then (for more than about 50 h reaction), the reaction rate decreased sharply and the amounts of Al and B_4C consumed, as well as those of Al_3BC and AlB_2 produced, varied quasi-linearly with the square root of the reaction time (straight lines in Fig. 8).

Examination of the Al–B_4C reaction zone in cylinders heated for increasing times further revealed the following features. After 3 h reaction at 1000 K (Fig. 9a), a few large AlB_2 crystals ($d \approx 20$ μm) were found in the aluminium matrix, sometimes far from the B_4C particles; while numerous, but small, Al_3BC crystals ($d \approx 2$ μm) appeared in some places of the surface of the B_4C particles. After 6 h reaction (Fig. 9b), these Al_3BC crystals were a little bigger and much more numerous than after 3 h; while new AlB_2 crystals had grown in the aluminium matrix, always

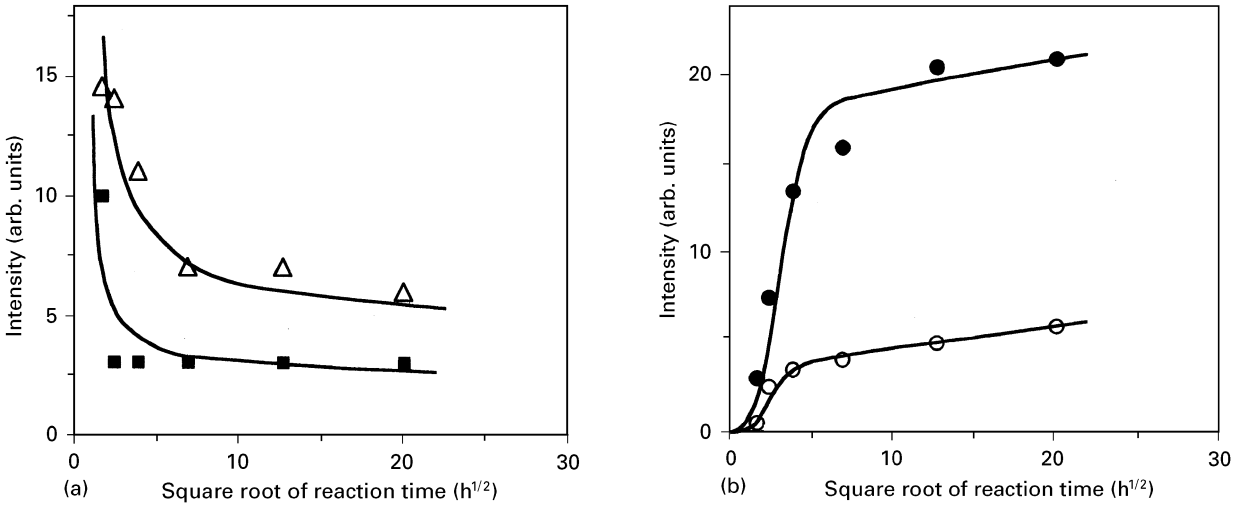

Figure 8 Dependence with time of the relative abundances of the reactants (△) Al and (■) B_4C (a) and of the products (●) Al_3BC and (○) AlB_2 (b) for Al–B_4C rods (Al:B:C = 40:48:12 at %) heat treated at 1000 K.

far from the Al–B_4C interface. Obviously, the B_4C particles were much more strongly attacked after 6 h reaction than after 3 h, suggesting that an incubation period may have passed before interaction between Al and B_4C effectively started. After 15 h reaction (Fig. 9c), the AlB_2 crystals in the aluminium matrix were still more numerous than after 6 h, while deep craters became visible in some places of the surface of the B_4C particles. In these places, aluminium was in direct contact with B_4C; whereas in other smoother places of the B_4C surface, the Al_3BC crystals tended to join together and form a quasi-continuous interfacial layer isolating B_4C from the metallic matrix. At a reaction time of 48 h (Fig. 9d), the B_4C particles exhibited very jagged outlines and were covered for the most part by a layer of Al_3BC crystals that appeared continuous, despite its very irregular thickness. For reaction times of 160 and 400 h (Fig. 9e and f), the thickness of the Al_3BC layer slightly increased and the B_4C particles tended to break into several chips, but the general morphologies of the samples remained the same as that observed after 48 h heating. It can be remarked that B_4C chips were still present after 400 h reaction at 1000 K (Fig. 9f), which indicated that once continuous, the Al_3BC layer very efficiently protected B_4C against aluminium attack.

Other experiments were realized on Al–B_4C rods (Al:B:C = 40:48:12 at %) and cylinders (Al:B:C =

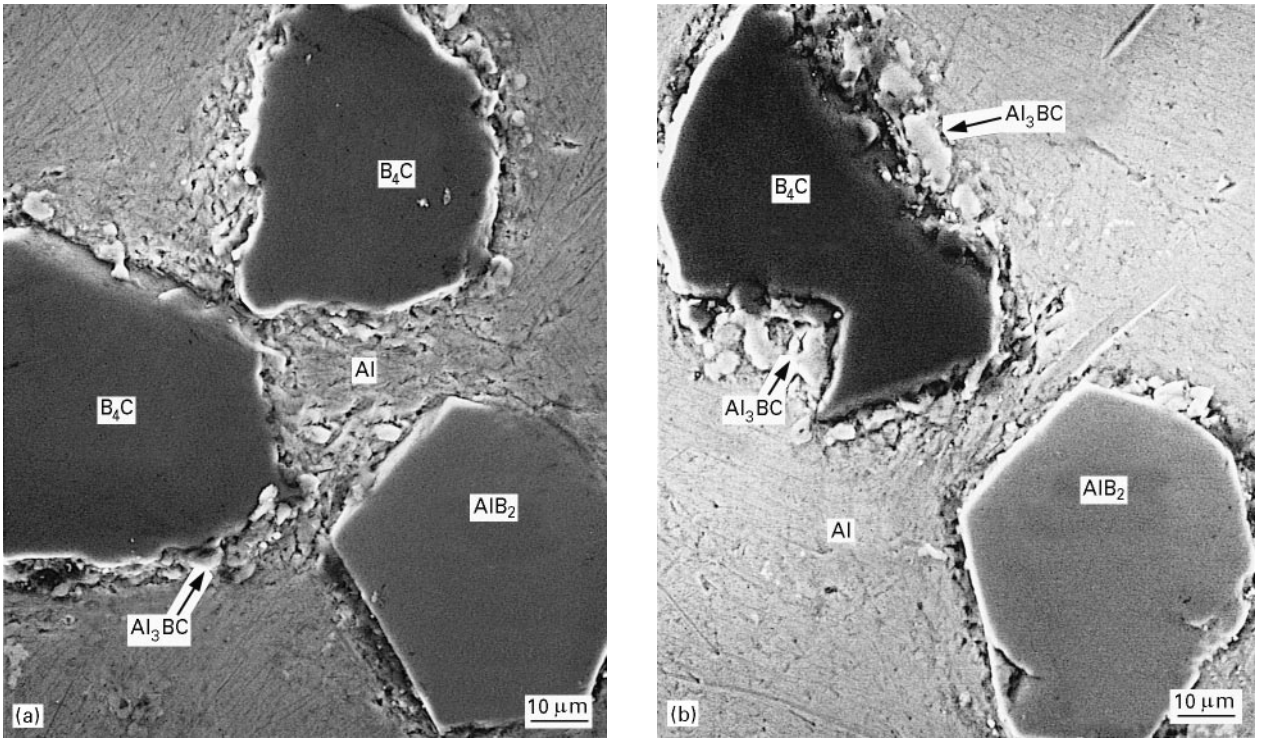

Figure 9 SEM photographs of Al–B_4C cylinders (Al:B:C = 95:4:1 at %) reacted at 1000 K for different times; (a) 3 h, (b) 6 h, (c) 15 h, (d) 48 h, (e) 160 h and (f) 400 h.

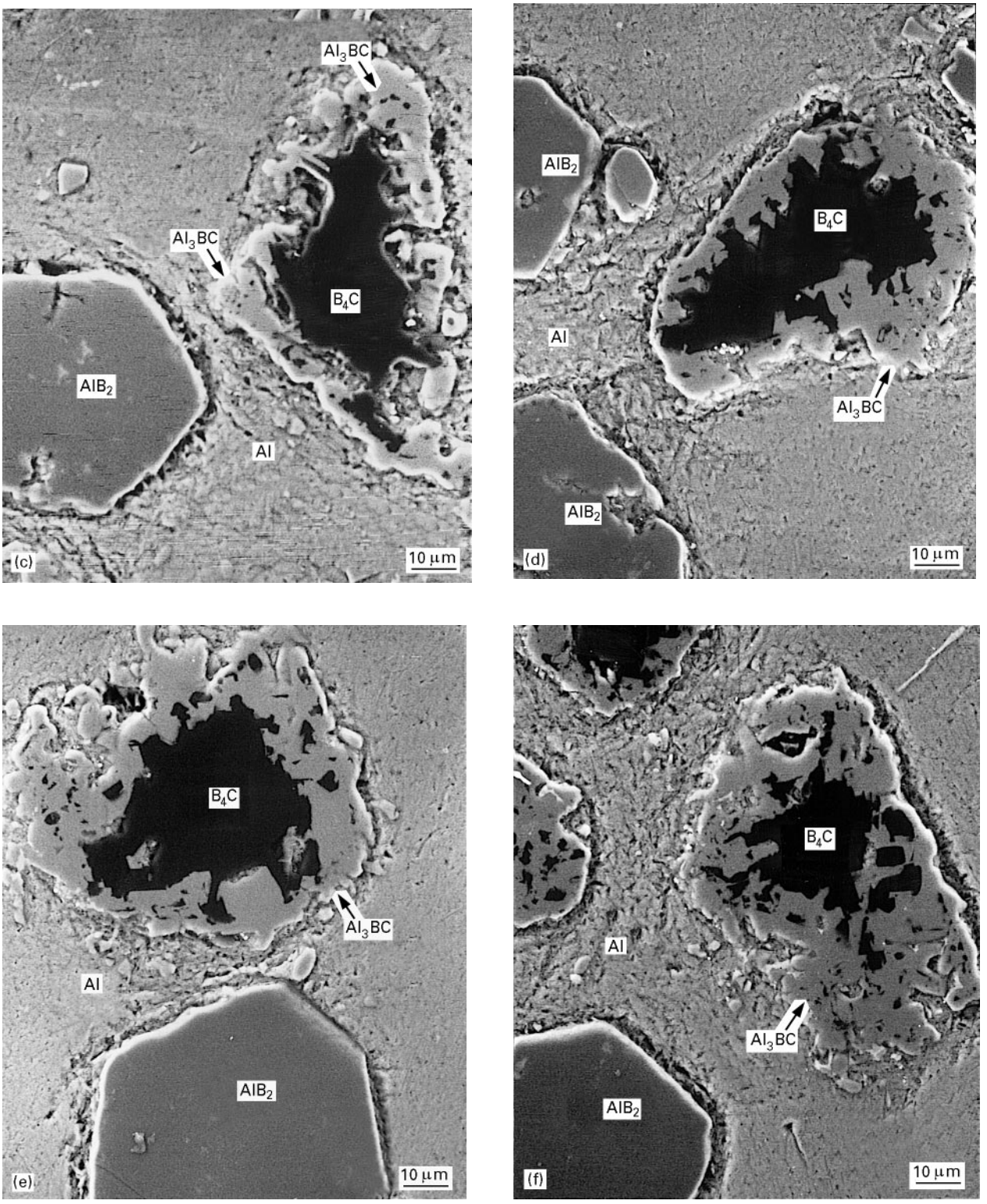

Figure 9 (continued).

95:4:1 at %) under the same conditions as previously, except for the heating temperature which was raised to 1200 K. At that temperature, decomposition of B_4C by liquid aluminium proceeded at a much faster rate than at 1000 K, as shown by the SEM photograph presented in Fig. 10. In fact, this photograph taken of an Al–B_4C cylinder heated for only 3 h at 1200 K reveals exactly the same morphological features as those previously exhibited by the series of samples heated at 1000 K, AlB_2 being simply replaced by $Al_3B_{48}C_2$ (β-AlB_{12}). More especially, it can be noted that the occurrence of a reaction is not obvious in some areas, while severe attack of B_4C is already visible in other places. This confirms the existence of a variable incubation period before reaction starts. In places where B_4C is strongly attacked, Al_3BC tends again to form a protective layer, continuous but very irregular in thickness, on a B_4C surface that has become very rough. For reaction times longer than 3 h, the major part of B_4C appeared to have decomposed into Al_3BC and $Al_3B_{48}C_2$ (β-AlB_{12}). However, B_4C fragments were still found after 160 h reaction at

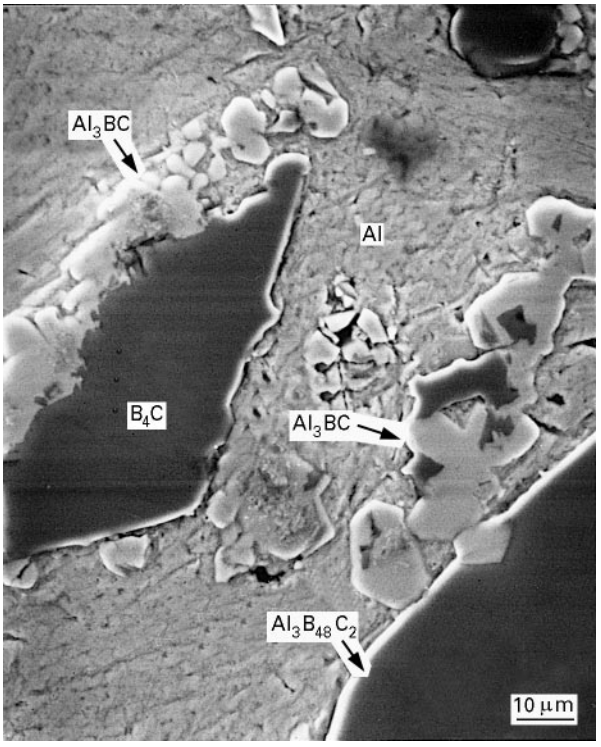

Figure 10 SEM photograph of an Al–B_4C cylinder (Al:B:C = 95:4:1 at %) reacted at 1200 K for 3 h.

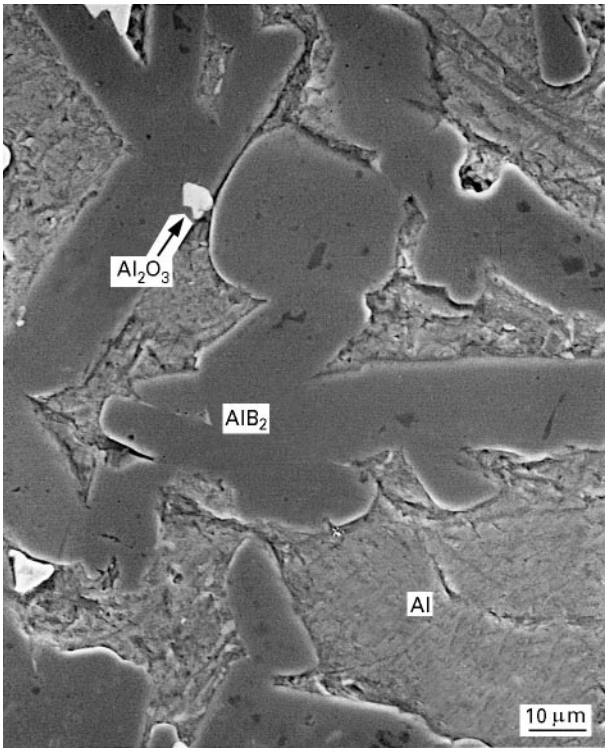

Figure 11 AlB_2 crystals grown in an Al–B mixture (50:50 at %) heated for 160 h at 1160 K.

1200 K, confirming that when continuous, the Al_3BC layer surrounding the B_4C particles constituted a very efficient diffusion barrier against liquid aluminium attack.

3.4. Complementary experiments

It has been shown in Section 3.1. that the products of chemical interaction between aluminium and boron carbide (B_4C) were Al_3BC and either AlB_2 or $Al_3B_{48}C_2$ (β-AlB_{12}), AlB_2 being formed at temperatures lower than or equal to 1100 K and $Al_3B_{48}C_2$ (β-AlB_{12}) at 1150 K or above. A new series of isothermal diffusion experiments was undertaken to define more precisely the temperature at which $Al_3B_{48}C_2$ (β-AlB_{12}) replaced AlB_2 and to relate this transition temperature with the thermal decomposition of AlB_2. For these purposes, Al–B and Al–B_4C mixtures with respective compositions of Al:B = 50:50 at % (points 13–20 in Fig. 1) and Al:B:C = 40:48:12 at % (points 13′–20′ in Fig. 1) were cold pressed in the form of small rods, heat treated for 110–160 h under 10^5 Pa of argon in the temperature range 1100–1200 K and characterized after rapid cooling. For better accuracy, each experiment was realized by heating together in the same alumina boat an Al–B rod and an Al–B_4C rod.

The results summarized in Table V clearly indicate that the replacement of AlB_2 by $Al_3B_{48}C_2$ (β-AlB_{12}) as a reaction product of the chemical interaction between liquid aluminium and B_4C occurs at a temperature of 1141 ± 4 K; whereas in the Al–B binary system and under 10^5 Pa, AlB_2 is stable up to a temperature of 1165 ± 5 K. Figs 11 and 12 show the two sorts of crystals, AlB_2 and α-AlB_{12}, as they appeared in Al–B mixtures heated for 160 h at 1160 and 1170 K, respectively.

Another series of experiments was performed with the aim of acquiring a more general view of the phase

TABLE V Phases formed in Al–B mixtures (Al:B = 50:50 at %) and Al–B_4C mixtures (Al:B:C = 40:48:12 at %) reacted for 110–160 h at different temperatures

Experiment no.	Temperature (K)	Phases characterized after heat treatment	
		Al–B mixtures	Al–B_4C mixtures
13; 13′	1100	–	Al, B_4C, Al_3BC, AlB_2
14; 14′	1125	Al, AlB_2	Al, B_4C, Al_3BC, AlB_2
15; 15′	1137	Al, AlB_2	Al, B_4C, Al_3BC, AlB_2
16; 16′	1145	Al, AlB_2	Al, B_4C, Al_3BC, $Al_3B_{48}C_2$
17; 17′	1150	Al, AlB_2	Al, B_4C, Al_3BC, $Al_3B_{48}C_2$
18; 18′	1160	Al, AlB_2	Al, B_4C, Al_3BC, $Al_3B_{48}C_2$
19; 18′	1170	Al, α-AlB_{12}	–
19; 19′	1200	Al, α-AlB_{12}	–

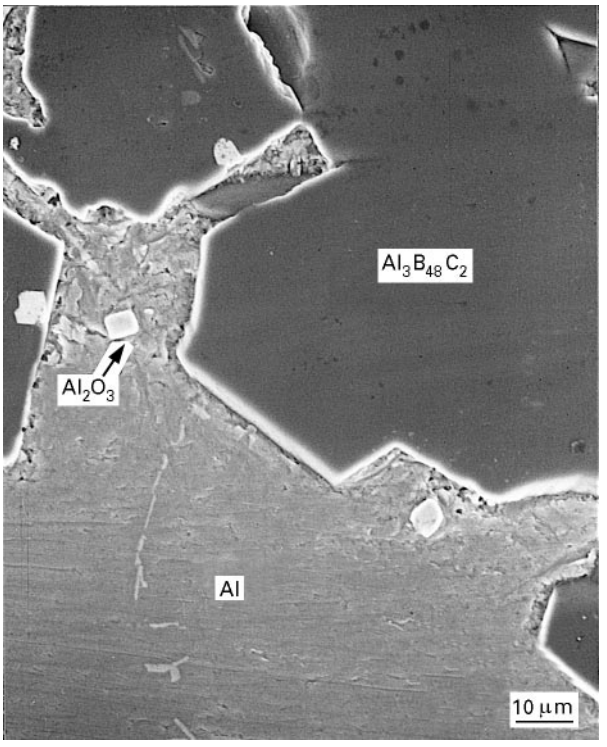

Figure 12 α-AlB_{12} crystals grown in an Al–B mixture (50:50 at %) heated for 160 h at 1170 K.

relations in the Al–B–C ternary system at 1273 K. For that purpose, powder mixtures with compositions located in the Al–B–C triangle, but out of the Al–B_4C line, were cold pressed, heat treated for 160 h at 1273 K and characterized by XRD after rapid cooling.

From the results summarized in Table VI, it appears that equilibrium has been reached only for mixtures prepared from the elements and having initial compositions lying in the Al-rich corner o the Al–B–C triangle, i.e. mixtures 21–25 (Fig. 1, Table VI). These mixtures are in effect the only ones to contain three phases or less (Al_2O_3 impurity excepted), which is the necessary condition to satisfy the phase rule in a ternary system under a constant pressure and at a temperature fixed a priori (the coexistence of four phases is not theoretically impossible but it is very unlikely because it would suppose that the temperature fixed a priori exactly corresponds to an invariant transformation). Consequently, the only phase equilibria whose existence can be considered as experimentally well established in the Al–B–C isothermal section at 1273 K are the solid–liquid (L) equilibria: Al_4C_3–L, Al_3BC–L, $Al_3B_{48}C_2$–L, Al_4C_3–Al_3BC–L and Al_3BC–$Al_3B_{48}C_2$–L. As α-AlB_{12} is in equilibrium with an Al-rich liquid in the Al–B binary system at 1273 K, a third three-phased solid–liquid equilibrium α-AlB_{12}–$Al_3B_{48}C_2$–L must also exist. For all other mixtures listed in Table VI, results obtained at the end of the heat treatment were not clear: if any, reactions progressed at too slow a rate and equilibrium was too far to be reached. In such a situation, definitive conclusions could not be drawn. In particular, it was not possible to decide whether B_4C was in equilibrium with Al_3BC or not, although a crossed-reaction was tried (experiment 26). Just such an indication was given by the results of experiments 27–29 for the possible existence of the three-phased triangles C–Al_4C_3–$Al_8B_4C_7$, C–B_4C–$Al_8B_4C_7$ and $Al_8B_4C_7$–Al_3BC–Al_4C_3.

Finally, an Al–B_4C rod (Al:B:C = 40:48:12 at %) was first treated in a conventional tubular furnace under 10^5 Pa of argon for 160 h at 1273 K and then reheated by electron bombardment under 10^{-2} Pa to about 1800 K (temperature determined by pyrometry to $\pm$ 150 K). At the end of the first treatment at 1273 K, Al, Al_3BC and $Al_3B_{48}C_2$ were the major constituents of the sample (only traces of B_4C remained). After reheating near 1800 K, it was no longer possible to characterize Al_3BC and $Al_3B_{48}C_2$ by XRD and the sample mainly consisted of Al and of a B_4C-type phase. Repeating the experiment a second time gave the same results. The existence of an equilibrium between B_4C and liquid Al near and above 1800 K appeared to be very likely.

4. Discussion

In the course of the above-reported experimental study, information of different kinds was collected. We will now try to bring together these elements and point out the general principles governing the Al–B_4C interface chemistry. After some preliminary considerations, we will interpret the results of Al–B_4C mixtures in terms of kinetics and reaction mechanism. To conclude, we will examine the thermodynamic aspect of this chemical interaction.

TABLE VI Phases characterized by XRD in mixtures of the Al–B–C system reacted for 160 h at 1273 K

Experiment no.	Reactants	Al:B:C initial composition (at %)	Phases characterized by XRD after reaction
21	Al, B, C	65:10:25	Al, Al_3BC, Al_4C_3, (Al_2O_3)
22	Al, B, C	80:9:11	Al, Al_3BC, Al_4C_3, (Al_2O_3)
23	Al, B, C	80:10:10	Al, Al_3BC, (Al_2O_3)
24	Al, B, C	80:11:9	Al, Al_3BC, $Al_3B_{48}C_2$, (Al_2O_3)
25	Al, B, C	50:42:8	Al, Al_3BC, $Al_3B_{48}C_2$, (Al_2O_3)
26	Al_4C_3, B	27:53:20	Al_4C_3, B
27	Al, B, C	40:10:50	C, Al_4C_3, Al_3BC, $Al_8B_4C_7$
28	Al, B, C	15:45:40	C, Al_3BC, Al_4C_3, $Al_8B_4C_7$
29	Al_4C_3, B_4C	29:40:31	Al_4C_3, B_4C, $Al_8B_4C_7$ (traces)

4.1. General considerations

It is clear from all the experimental results obtained in this work that B_4C decomposes by chemical interaction with solid or liquid aluminium at any temperature ranging from 900 to at least 1273 K. The reaction products are the ternary carbide Al_3BC and either the diboride AlB_2 or the complex borocarbide $Al_3B_{48}C_2$ (β-AlB_{12}), according to whether the temperature is lower than or higher than 1141 ± 4 K (temperature determined in Section 3.4.). It must be emphasized that, to the detection limit of the techniques used, no trace of the aluminium carbide Al_4C_3 was found. This is a specific feature that differentiates the Al–B_4C couple from other reactive couples such as Al–TiC [34] or Al–SiC [35, 36] at the interface of which Al_4C_3 appears as a major reaction product.

4.2. Mechanism and kinetics of the decomposition of B_4C by aluminium attack

Referring to the results obtained after heating Al–B_4C mixtures for varying times at 1000 K (Section 3.3.), the main steps of the decomposition of B_4C by liquid aluminium at this temperature can be described as follows.

After an incubation period that very likely corresponds to the breakage of the oxide films initially present at the surface of Al and B_4C (Al_2O_3, B_2O_3, . . .), a true Al–B_4C interface is created at some points. At these points, the metal rapidly saturates in boron and carbon by simple dissolution of the carbide. As the maximum solubilities of these elements in aluminium are very low, at the order of 1000 and of a few tenths of at ppm at 1000 K, respectively [18, 37], this simple dissolution process ends very quickly. It is immediately followed by the nucleation and growth of Al_3BC and AlB_2 crystals from an aluminium matrix supersaturated in carbon and boron. The nuclei of Al_3BC and AlB_2 do not form, however, at the same rate and in the same places: Al_3BC easily nucleates at the surface of B_4C, whereas AlB_2 nucleates with difficulty and is only present in the metal matrix, very likely on Al_2O_3 impurity seeds.

Once this stage is arrived at, interaction progresses via a classical dissolution–precipitation mechanism, a detailed description of which is given in [36] and deals with high-temperature interaction at the Al–SiC interface. In the present case, carbon and boron atoms migrate by liquid-phase diffusion from the surface of B_4C where aluminium supersaturates in carbon and boron (dissolution) to faces of Al_3BC and AlB_2 crystals that are growing from the metal (precipitation). In places where Al_3BC crystals are fixed and begin to grow, B_4C is protected against further attack; while in places where liquid aluminium remains in direct contact with the surface of B_4C, dissolution continues. This gives rise to the formation of deep dissolution craters at the B_4C surface and the surface becomes rougher and rougher: such a crater is visible between the Al_3BC crystals on the SEM photograph presented in Fig. 13. Other reasons that may contribute to an increase in roughness of the surface of B_4C and to the subsequent fragmentation of this carbide in small pieces are an incubation time variable from one point to another, poor wetting by liquid aluminium, and preferential attack in certain crystallographic orientations or at the grain boundaries.

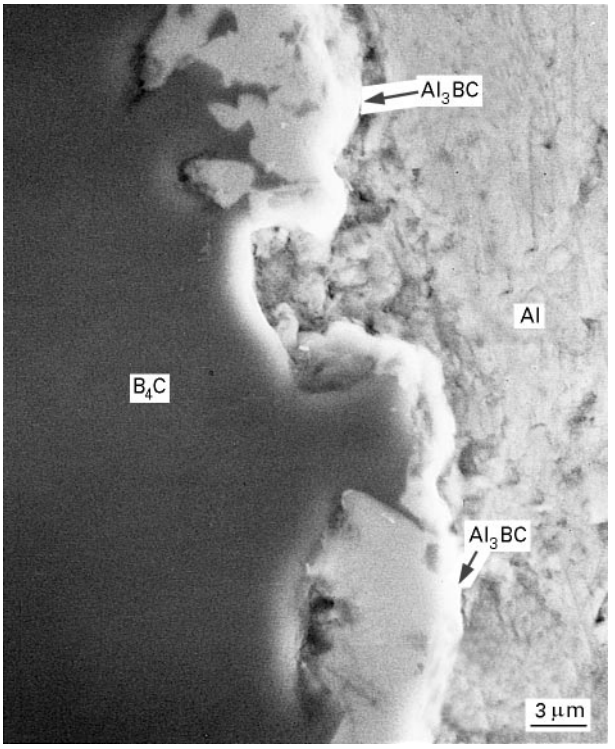

Figure 13 Detailed view (SEM) of the Al–B_4C interface after 15 h reaction at 1000 K.

It can easily be understood that as long as an important part of the B_4C surface is directly exposed to aluminium, the amount of B_4C dissolved increases quasi-linearly with reaction time. As indicated by the XRD results reported in Fig. 8a and b, such a situation prevails for the first 15 h of reaction at 1000 K. This is no more true when the growing Al_3BC crystals tend to join together and form a dense layer at the B_4C surface. Except for some rare places where the metal is still in direct contact with B_4C, decomposition of this carbide by the above-described dissolution–precipitation mechanism is no longer possible. At this stage, further growth of reaction product crystals (Al_3BC and AlB_2) must obey another mechanism that implies solid state diffusion of B, C or Al atoms through the growing Al_3BC layer. In this last passivation step where solid state diffusion through the Al_3BC layer has become rate controlling, the rate at which B_4C decomposes decreases considerably and the amounts of reactants consumed and of reaction products formed at a given temperature tend to vary proportionately to the square root of the reaction time, according to the XRD results reported in Fig. 8. In fact, it appears from these XRD results and from the SEM observations reported in Fig. 9 (general evolution) and in Fig. 13 (detailed view) that Al_3BC acts as a very efficient diffusion barrier at the Al–B_4C interface.

This reaction mechanism derived from the results obtained at 1000 K and including an incubation

period, the saturation of the metal in B and C, the growth by dissolution–precipitation of Al_3BC and of a C-poor boride, and finally the passivation of B_4C by Al_3BC, can be generalized for the entire temperature range of 900–1273 K. Effectively, samples heated at 920, 1200 or 1273 K exhibited the same morphological features as those reacted at 1000 K, with large C-poor boride crystals grown in the metal matrix and a rough B_4C surface covered by a layer of Al_3BC crystals. In this regard, it is worth noting that $Al_3B_{48}C_2$ plays exactly the same role at temperatures higher than 1141 K as AlB_2 at temperatures lower than 1141 K.

4.3. Phase equilibria in the Al–B–C ternary system

Attempts made to relate the results obtained in this study with the phase equilibria that might exist in the Al–B–C system at 1273 K or below have resulted in the tentative representations of the Al–B–C phase diagram given in Figs 14 and 15. In these figures, the bold lines represent phase equilibria that can be considered as non-ambiguously established and the thin lines as phase equilibria whose existence can only be assumed on the basis of some experimental indications or theoretical considerations.

Under this convention, the solid–liquid phase equilibria at 1273 K in the Al–B–C system (Fig. 14) appear as bold lines. Effectively, these equilibria derive from clear results detailed in Section 3.4. They are, moreover, coherent with all observations made at 1273 K such as, for example, the crystallization of Al_3BC and $Al_3B_{48}C_2$ from an Al-rich liquid and the fact that these three phases remain as major constituents in an Al–B_4C mixture (Al:B:C = 40:48:12 at %) reacted for 160 h at 1273 K (Fig. 6). As for the solid–solid phase equilibria at 1273 K, they are represented by thin lines because the results of the experiments made were not probative. In fact, it appears in Section 3.4. that determination of such solid state equilibria at 1273 K is practically impossible by classical isothermal diffusion experiments, due to too low reaction kinetics. The tentative representation of these solid–solid equilibria given in Fig. 14 is only based on indications obtained in experiments 23 and 24 (Section 3.4., Table VI) and on the fact that no intermediate phase has been characterized at the Al_3BC/B_4C interface, neither in the present work nor in a previous investigation by high resolution electron microscopy [33]. It can be noticed that such a set of solid–solid phase equilibria supposes that the ternary phase $AlB_{24}C_4$ (AlB_{10}) is unstable at or below 1273 K.

When the temperature decreases from 1273 K, several invariant transformations involving an Al-rich liquid occur in the Al–B–C ternary system and in the Al–B and Al–C binary subsystems. They correspond to the different points marked on the polythermal liquidus projection schemed in Fig. 15.

Two of these transformations have been studied in detail in Section 3.4. The first one, represented by point p_1 in Fig. 15, is a peritectic reaction in the Al–B binary subsystem. This transformation, which can be

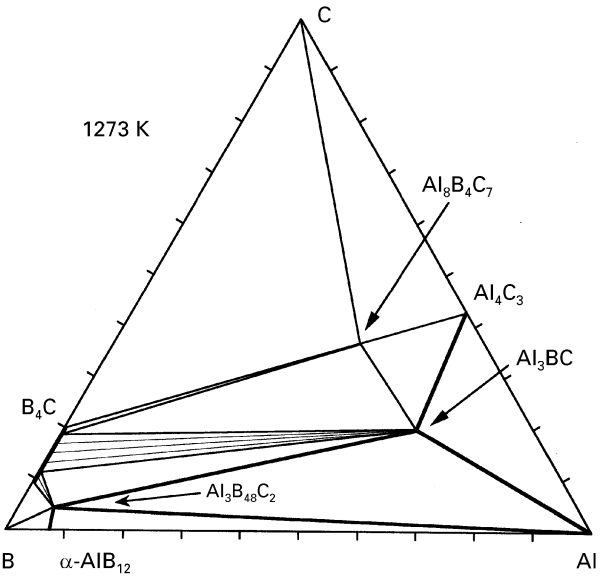

Figure 14 The Al–B–C isothermal section at 1273 K, as constructed from the experimental results of the present work. Bold lines represent liquid–solid equilibria non-ambiguously established; thin lines represent solid–solid equilibria the existence of which appears probable but could not be clearly determined.

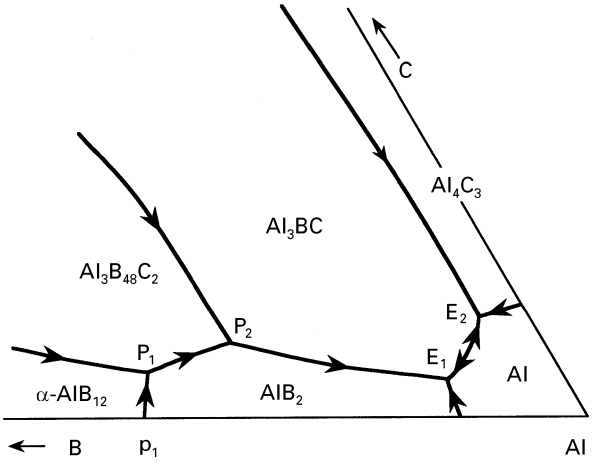

Figure 15 Al-rich corner of the Al–B–C phase diagram: tentative polythermal liquidus projection.

written as

$$\alpha\text{-}AlB_{12} + L \Leftrightarrow AlB_2 \qquad (1)$$

has been found to occur at 1165 ± 5 K. It is worth noting that this value of 1165 ± 5 K is much lower than the temperatures generally reported in the literature for the peritectic decomposition of AlB_2: about 1200 K [38], 1248 K [39] or 1303 K [18]. These large differences are very likely due to the fact that the temperatures previously reported were measured on heating by differential thermal analysis (DTA), whereas our determination has been made by isothermal diffusion. For rapid transformations, both techniques generally yield the same results. Now, for a transformation that proceeds at a slow rate, which is effectively the case for the decomposition of AlB_2, the transformation temperature measured by DTA will shift towards higher values (the shift varying with the

heating rate) while that determined by isothermal diffusion experiments will remain unaffected. As an example, for an invariant transformation in the Al–C–Ti system proceeding at a slow rate and involving liquid aluminium, TiC, Al_4C_3 and Al_3Ti, we found a temperature of 1085 K by isothermal diffusion whereas DTA yielded an erroneous value of 1187 K (102 K shift) on heating at a rate of 4 K min^{-1} [34].

The second transformation involving an Al-rich liquid investigated in Section 3.4. is a quasi-peritectic reaction in the Al–B–C ternary system that can be written as

$$Al_3B_{48}C_2 + L \Leftrightarrow AlB_2 + Al_3BC \qquad (2)$$

This transformation, represented by point P_2 in Fig. 15, occurs at a fixed temperature of 1141 ± 4 K (under a pressure of 10^5 Pa). From thermodynamic considerations, the existence of the two former transformations implies that of a third transformation between 1165 and 1141 K. On account of the fact that carbon is insoluble in AlB_2 and assuming that no ternary eutectic exists between the phase L, AlB_2, α-AlB_{12} and $Al_3B_{48}C_2$, this third transformation represented by point P_1 (Fig. 15) cannot be other than a quasi-peritectic reaction in which an Al-rich liquid reacts with α-AlB_{12} to give $Al_3B_{48}C_2$(β-AlB_{12}) and AlB_2 according to the equation

$$\alpha\text{-}AlB_{12} + L \Leftrightarrow Al_3B_{48}C_2 + AlB_2 \qquad (3)$$

It can be seen in Fig. 15 that Equation 2 gives rise to a descending monovariant line corresponding to the equilibrium AlB_2–Al_3BC–L. Another descending monovariant line representing the equilibrium Al_3BC–Al_4C_3–L (established at 1273 K) also exists. It has been assumed that these two descending lines end in two eutectic points (points E_1 and E_2 in Fig. 15) that would correspond, in the Al–B–C ternary system, to the two invariant reactions

$$L \Leftrightarrow AlB_2 + Al_3BC + Al_s \qquad (4)$$

$$L \Leftrightarrow Al_4C_3 + Al_3BC + Al_s \qquad (5)$$

Under such hypotheses, which are very difficult to verify experimentally, the Al–Al_3BC section would appear as quasi-binary, the monovariant line E_1E_2 passing through a maximum.

5. Conclusions

The aim of the present study was to obtain a better insight into the interface chemistry of the Al–B_4C couple. The results of the isothermal diffusion experiments that have been carried out have determined new elements for a better understanding of this chemistry. More especially, the nature, the abundance and the morphology of the phases formed by chemical reaction at temperatures lower than or equal to 1273 K have been characterized, reaction mechanisms have been elucidated and liquid–solid phase equilibria have been established.

Some questions remain, however, unsolved concerning the solid–solid phase equilibria in the Al–B–C system. Due to too low reaction kinetics, experimental determination of such equilibria at medium or low temperatures has appeared very difficult and only hypotheses can be advanced. It is thought that progresses in this field may arise from indirect approaches combining experiments such as high temperature cross-reactions and heat capacity measurements with thermodynamic calculations.

Acknowledgements

The authors gratefully acknowledge the CMEABG, Université Lyon 1, where characterizations by SEM and EPMA could be realized.

References

1. F. THEVENOT and M. BOUCHACOURT, *L'industrie Céramique* **732** (1979) 655.
2. C. J. BEIDLER, W. E. HAUTH and A. GOEL, *J. Test. Eval.* **20** (1992) 67.
3. W. KAI, J. M. YANG and W. C. HARRIGAN, *J. Script Metall.* **23** (1989) 1277.
4. D. C. HALVERSON, A. J. PYSIK, I. A. AKSAY and W. E. SNOWDEN, *J. Amer. Ceram. Soc.* **72** (1989) 775.
5. A. J. PYZIK and D. R. BEAMAN, *ibid.* **78** (1995) 305.
6. N. LERNER, L. BAUM, N. SHAFRY and D. G. BRANDON, *Mater. Sci. Monogr.* **68** (1991) 189.
7. J. LECOMTE-BECCKERS and E. DIDERRICH, *ATB Metall.* **27** (1987) 3.
8. J. BOUIX, C. VINCENT, H. VINCENT and R. FAVRE, in "Chemical vapor deposition of refractory metals and ceramics", MRS Symposium Proceedings, Vol. 168, edited by T. M. Besman and B. M. Gallois (Materials Reseach Society, Pittsburgh, PA, 1990) p. 305.
9. H. VINCENT, B. BONNETOT, J. BOUIX, H. MOURICHOUX and C. VINCENT, *J. Phys.* **50** (1989) 249.
10. H. VINCENT, C. VINCENT, H. MOURICHOUX J. P. SCHARFF and J. BOUIX, *Carbon* **30** (1992) 495.
11. C. VINCENT, H. VINCENT, H. MOURICHOUX and J. BOUIX, *J. Mater. Sci.* **27** (1992) 1892.
12. H. VINCENT, C. VINCENT, M. P. BERTHET, J. BOUIX, and G. GONZALES, *Carbon* **34** (1996) 1041.
13. P. DORNER, PhD thesis, Institüt für Metallkunde der Universität, Stuttgart (1982).
14. T. A. CHERNYSHOVA and A. V. REBROV, *J. Less-Common Metals.* **117** (1986) 203.
15. J. C. VIALA, G. GONZALEZ and J. BOUIX, *J. Mater. Sci. Lett.* **11** (1992) 711.
16. G. GONZALEZ, C. ESNOUF and J. C. VIALA, *Mater. Sci. Forum* **126–128** (1993) 125.
17. G. GONZALEZ, PhD thesis, INSA de Lyon, Lyon (1993).
18. H. DUSCHANEK and P. ROGL, *J. Phase Equil.* **15** (1994) 543.
19. H. L. LUKAS, in "Ternary alloys", Vol. 3, edited by G. Petzow and G. Effenberg (VCH Verlags, Weinheim, 1990) p. 140.
20. G. A. JEFFREY and V. Y. WU, *Acta Crystallogr.* **20** (1966) 538.
21. L. L. ODEN and R. A. McCUNE, *J. Amer. Ceram. Soc.* **73** (1990) 1529.
22. G. WILL and K. H. KOSSOBUTZKI, *J. Less-Common Metals* **44** (1976) 87.
23. M. BOUCHACOURT and F. THEVENOT, *ibid.* **82** (1981) 219.
24. V. I. MATKOVICH, J. ECONOMY, R. F. GIESE Jr, *J. Amer. Chem. Soc.* **86** (1964) 2337.
25. J. S. KASPER, M. VLASSE and R. NASLAIN, *J. Solid State Chem.* **20** (1977) 281.
26. I. IGASHI, T. SAKURAI and T. ATODA, *ibid.* **20** (1977) 61.
27. V. I. MATKOVICH, R. F. GIESE and J. ECONOMY, *Z. Kristall.* **122** (1965) 108.
28. J. A. KOHN, G. KATZ and A. A. GIARDINI, *ibid.* **111** (1958) 53.

29. R. F. GIESE Jr, J. ECONOMY and V. I. MATKOVICH, *Acta Crystallogr.* **20** (1966) 697.
30. Z. INOUE, H. TANAKA and Y. INOMATA, *J. Mater. Sci.* **15** (1980) 3036.
31. R. J. OSCROFT, P. H. A. ROEBUCK and D. P. THOMPSON, *Brit. Ceram. Trans.* **94** (1995) 25.
32. A. LIPP and M. RODER, *Z. Anorg. Allgem. Chem.* **343** (1966) 1.
33. M. SARIKAYA, T. LAOUI, D. L. MILIUS and I. A. AKSAY, in Proceedings of the 45th Annual Meeting of the Electron Microscopy Society of America, edited by G. W. Bailey (San Francisco Press, CA 1987) p. 168.
34. J. C. VIALA, C. VINCENT, H. VINCENT and J. BOUIX, *Mater. Res. Bull.* **25** (1990) 457.
35. J. C. VIALA, P. FORTIER and J. BOUIX, *J. Mater. Sci.* **25** (1990) 1842.
36. J. C. VIALA, F. BOSSELET, V. LAURENT and Y. LEPETITCORPS, *ibid.* **28** (1993) 5301.
37. C. J. SIMENSEN, *Metall. Trans. A* **20** (1989) 191.
38. L. F. MONDOLFO, in "Aluminum alloys: structure and properties" (Butterworth, London, 1976) p. 228.
39. T. B. MASSALSKI, in "Binary Alloy Phase Diagrams", Vol. 1 (American Society for Metals, Metals Park, OH, 1986) p. 91.

Received 30 July 1996
and accepted 26 February 1997